Characterization and Application of Natural Photosensitizer and Poly(vinylidene Fluoride) Nanofiber Membranes-Based Electrolytes in DSSC

Nafisatus Zakiyah[1], Nita Kusumawati[1*], Pirim Setiarso[1], Supari Muslim[2], Qurrota A'yun[1], and Marinda Mayliansarisyah Putri[1]

[1]*Department of Chemistry, Faculty of Mathematics and Natural Sciences, Universitas Negeri Surabaya, Jl. Ketintang, Surabaya 60231, Indonesia*

[2]*Department of Electrical Engineering, Faculty of Engineering, Universitas Negeri Surabaya, Jl. Ketintang, Surabaya 60231, Indonesia*

* ***Corresponding author:***

email: nitakusumawati@unesa.ac.id

Received: July 1, 2023
Accepted: December 5, 2023

DOI: 10.22146/ijc.86386

Abstract: *This comprehensive research has explored the potential of enhancing dye-sensitized solar cells (DSSC) by harnessing environmentally friendly natural dyes, such as chlorophyll pigments from pandanus (664.1 nm) and papaya leaves (664.0 nm), as well as betacyanin pigments from sappan-mangosteen (536.2 nm). Electrochemical analyses elucidated the energy band gaps, revealing a hierarchy with the smallest band gap observed for papaya leaves (1.387 eV), followed closely by sappan-mangosteen (1.389 eV) and pandan leaves (1.396 eV). This research effectively addressed the persistent issue of electrolyte leakage in DSSC development by introducing a polymer electrolyte derived from polyvinylidene fluoride (PVDF) through electrospinning and phase inversion techniques. SEM characterization results and thermogravimetric analysis underscored the superior characteristics and high thermal stability of the PVDF nanofiber polymer for DSSC applications. The study's pivotal findings underscore the remarkable DSSC performance achieved with chlorophyll pigment from papaya leaves, reaching 1.31% efficiency without a polymer electrolyte. Moreover, the sappan-mangosteen dye emerged as a promising contender with the highest efficiency values when applied with polymer electrolyte, recording rates of 1.17% for PVDF NF and 0.95% for PVDF, which are notably comparable to the efficiency of liquid electrolyte at 1.26%.*

Keywords: *DSSC; photosensitizer; natural dyes; polymer electrolyte*

■ INTRODUCTION

The surge in global population, combined with industrial expansion and technological advancements, has resulted in a continually growing demand for energy [1]. To address the pressing issues of escalating global energy consumption and the environmental repercussions associated with the burning of fossil fuels, the scientific community has emphasized the critical need for renewable energy development [2-3]. Solar energy is one of the most promising renewable energy sources, offering the potential to be converted into electricity by photovoltaic modules. Several types of solar cells have been developed, including silicon-based, thin-film amorphous, organic, and dye-sensitized solar cells (DSSCs) [4]. DSSCs have garnered significant attention from researchers due to their attributes such as thin-film construction, high efficiency, straightforward fabrication, and environmentally friendly processing [5-6]. DSSCs typically consist of two conducting glass substrates and three crucial components: a porous semiconductor with a band gap sensitive to dye molecules, a counter electrode, and a redox electrolyte [7-9].

The performance of DSSC relies heavily on the choice of the sensitizer dye employed. Research has identified ruthenium as one of the most efficient and stable photosensitizers [1]. Nonetheless, the expense and heavy metal composition of these dyes contribute to environmental pollution concerns [5]. In response,

natural dyes derived from plant extracts have emerged as an appealing alternative to ruthenium dyes, offering cost-effectiveness, environmental friendliness, biodegradability, ease of preparation, and abundant availability [10]. Commonly employed natural pigments include brazilin, chlorophyll, anthocyanins, carotenoids, betalains, flavonoids, cyanine, and tannins [5].

In the realm of DSSC components, the electrolyte plays a pivotal role. It is responsible for facilitating the transfer of internal charge carriers between electrodes and metal oxides [11]. While liquid electrolytes typically provide higher efficiency than gels and solid counterparts, they come with inherent drawbacks, such as seal leakage, solvent evaporation, iodine sublimation, short-term stability, dye desorption, and corrosion of the opposing electrode [12]. As an alternative approach, polymer-based electrolytes present distinct advantages, including high ionic conductivity, tensile strength, flexibility, safety, ease of fabrication, and leak resistance [13].

In the context of this study, the chosen polymer for the electrolyte is polyvinylidene fluoride (PVDF), notable for its exceptional electrochemical stability as an electrolyte solution and superior mechanical strength when compared to alternatives like polyethylene oxide (PEO), polyacrylonitrile (PAN), polyurethane (PU), and polyvinyl chloride (PVC) [14-15]. However, it is important to note that PVDF is hydrophobic, which can potentially impede the ionic mobility of I^-/I_3^- ions within PVDF immersed in the electrolyte [15]. To enhance the mobility of the ions, a PVDF nanofiber membrane is employed in the fabrication of a quasi-solid electrolyte (gel) and solid electrolyte through the electrospinning method [10].

Considering the challenges concerning the stability of DSSC, particularly to the electrolytes, this research endeavors to address these issues through the development of polymer electrolytes employing PVDF and PVDF nanofibers (NF) within a liquid electrolyte matrix. The introduction of electrolyte variations aims to elucidate the effects of these variations on DSSC efficiency. To comprehensively understand the structural and property characteristics of the membranes, Fourier transform infrared (FTIR) spectroscopy is employed, shedding light on the intricate interactions among ions, polymers, solvents, and electrolytes. Simultaneously, differential scanning calorimetry (DSC) is utilized to delineate thermal transitions within the system. Further insights into the morphology of the PVDF membrane are gleaned through scanning electron microscopy (SEM).

Each DSSC series is meticulously assembled, utilizing natural dyes derived from a variety of plant extracts in combination with diverse types of electrolytes. The evaluation of the most efficient natural dyes for DSSC applications is contingent on an array of electrical testing parameters, encompassing measurements of current and voltage using a multimeter, wavelength assessments via a UV-vis spectrophotometer, and bandgap energy determinations derived from cyclic voltammetry measurements. This multifaceted approach is undertaken to enhance the stability and efficiency of DSSC, and to advance sustainable and environmentally friendly energy solutions.

■ EXPERIMENTAL SECTION

Materials

The materials used in this study, PVDF, acetone (≥ 99.5% purity), propylene carbonate (99.7% purity), anhydrous EC (99% purity), TiO_2 (99.5% purity), iodine (≥ 99.8% purity), and HNO_3 (≥ 99.9% purity), were purchased from Sigma Aldrich in Singapore. DMAC (≥ 99% purity), polyethylene glycol (PEG 1000), and KI (≥ 99% purity) were obtained from Merck in Germany. Methanol (99.8% purity) and Tween 80 were purchased from PT. Smart Lab in Indonesia. FTO glass (resistivity 10 Ω) was purchased from XinYu Xu Tking Glass Co., L, China. *Carica papaya* L. leaves, *Pandanus amaryllifolius* leaves, and *Garcinia mangostana* L. peel were collected from Jember, Indonesia. *Caesalpinia sappan* L. bark was purchased from Tanikita, Indonesia.

Instrumentation

Several instruments are used for characterization, such as the Shimadzu UV-1800 UV-vis spectrophotometry for UV absorption spectrum analysis natural photosensitizer, Perkin Elmer Spectrum

Two FTIR spectrometers with total attenuation reflection mode (ATR) at 30 °C, Zeiss EVO MA-10 SEM, and Linseis STA PT-1000 DSC at 70–170 °C with a heating rate of 10 °C/min, respectively for analysis of infrared spectrum, surface morphology, and thermal stability of liquid electrolytes and PVDF and PVDF-NF membrane-based electrolytes. Furthermore, the current reduction and oxidation using Computrace 797 VA Metrohm Voltammetry is used for band gap analysis of natural photosensitizers. The sample solution used is Mix 20 mL of natural photosensitizer with 5 mL KCl 0.3%. DSSC efficiency is evaluated based on current and voltage measurement using Krisbow KW08-267 Multimeter with a resistance of 200 kΩ and a voltage of 200 mV, while to obtain the effect of ionic conductivity on J_{sc}, electron transport analysis was carried out, in particular the DSSC electrochemical interface resistance, uses Gamry reference 3000 electrochemical impedance spectroscopy (EIS) [16].

Procedure

PVDF membrane manufacturing

The manufacture of PVDF membranes was carried out by casting knife and electrospinning methods as previously conducted [16].

Natural photosensitizer

The production of organic photosensitizers through maceration in this study closely aligns with the methodology outlined in the research conducted by Kusumawati et al. [16], which employed a consistent maceration process with a 1:6 ratio of sample to solvent. Specifically, *C. papaya* L. leaves were macerated in methanol, while *P. amaryllifolius* leaves underwent maceration using ethanol. In contrast, *C. sappan* L. bark (secang) and *G. mangostana* L. peel (mangosteen) were macerated with distilled water and blended at a 2:1 dye ratio of secang to mangosteen. Following maceration, the resulting solutions underwent an evaporation process, concentrating the natural dye extracts. These concentrated natural dye extracts were then carefully stored in a controlled environment with temperatures ranging from 20 to 25 °C, ensuring their readiness for application in subsequent phases of the study.

Fabrication DSSC

The DSSC comprises these components: an FTO (fluorine-doped tin oxide) anode, an FTO cathode, a semiconductor (TiO_2), a natural dye, an electrolyte, and a counter electrode. A layer of TiO_2 paste was applied to the FTO anode, which had a 3 cm^2 active area using the doctor blade method and sintered at 450 °C for 1 h. The product obtained after sintering is immersed in 10 mL of natural dye for a duration of 24 h. The PVDF membrane that was printed by the casting and electrospinning method was cut with a length of 2 cm and a width of 1.5 cm. For 1 h, the membrane was submerged in 1 mL of electrolyte. The cathode FTO glass is coated with carbon from the 2B pencil. The DSSC circuit is composed of FTO/TiO_2/PVDF/Pt/FTO membranes [16].

Characterization

The morphology of the electro-spun polymer nanofiber membrane was observed by SEM Zeiss EVO MA-10. Using a Perkin Elmer Spectrum Two FTIR spectrometer, the sample's FTIR spectrum was acquired in ATR mode at ambient temperature. The UV-vis absorption spectra of the color pigments used in the DSSC were analyzed using a UV-vis instrument (Shimadzu UV-1800). Changes in the current and potential of the color pigment used for the DSSC were analyzed using a Voltammetry Instrument (797 VA Computrace Metrohm). A DSC (Linseis STA PT-1000) was utilized to obtain the thermograms for DSC analysis. The current measurement in the circuit is measured using a Multimeter (Krisbow KW08-267), performed at room temperature by flanking the electrolyte sample on the DSSC circuit using a crocodile clamp connected to a multimeter and directed at a resistance of 200 k and a voltage of 200 MV.

■ RESULTS AND DISCUSSION

Making Polymer Electrolyte

Electrolyte leakage is one of the main problems of DSSC fabrication. Most DSSCs are developed using liquid electrolytes, with problems of electrolyte leakage and evaporation. Electrolyte polymer is the solution to this problem by the concurrent electrolyte in it. PVDF is a polymer with excellent electrochemical stability, has

good thermal and chemical resistance, so it has the potential to be used as I/I_3^- ion mobility in DSSC systems. PVDF polymers are made in two variations, namely flat-sheet, and nanofiber.

Flat-sheet PVDF is made using the phase inversion method. The phase inversion method works on the principle of diffusion through an immersion solution in a non-solvent coagulation bath [16-18]. The diffusion process occurs between solvent and non-solvent, where the solvent component will evaporate from the impression solution and the non-solvent will penetrate the layer to produce a solidified membrane [19-21].

At this stage, PVDF membranes are made by dissolving in DMAc and acetone solvents, which have a slight difference in solubility parameter scale, namely 16.0 $Mpa^{1/2}$ for PVDF; 16.8 $Mpa^{1/2}$ and 13.0 $Mpa^{1/2}$ for acetone [22-23]. In the phase inversion method, the coagulation bath is filled with non-solvent in the form of water with a parameter difference of 25.2 $Mpa^{1/2}$ between DMAc and 28.3 $Mpa^{1/2}$ between acetone. The choice of non-solvent is important in this method because the diffusion of the non-solvent is the main component that can drive the process, so the resulting membrane must solidify [24].

Nanofiber PVDF was formed by the electrospinning method [25-26]. Nanofiber is a membrane that is suitable for use as an electrolyte trap with its advantages in the form of high porosity, wettability of the electrolyte, high surface area, and the ability to form long-distance channels as proton transport [27-28]. The PVDF solution to be electrospinning was prepared according to the research of Moshfeghian et al. [29] with a composition of 18% in DMAc solvent and acetone in a ratio of 3:2. The making of the 18% composition resulted from determining the best SEM results from the three variations of the composition used, namely 16, 18, and 20% wherein 16% produced membranes in the presence of beading fibers due to low concentrations, 18% compositions produced membranes with perfect fibers with no defects in fibers and beads, while high compositions yielded membranes with large numbers of beads around fibers that have decreased in size [30]. The density of the composition can increase the viscosity of a solution so that it can reduce the flexibility of the fiber and decrease the homogeneity of the dispersion, which has an impact on the appearance of beads on the fiber [29]. In addition, a composition that is too low causes the concentration range to be too low so that it is easy to form beads on the fiber [31].

UV-vis Analysis

The dye in DSSC has an important role in increasing the absorption of the visible light spectrum on TiO_2. Natural dyes have advantages over synthetic dyes because they are more readily available, require fewer chemical operations to extract, have a high absorption coefficient, are less expensive, non-toxic, and biodegradable [32]. To determine the potential of papaya leaves, pandan leaves, and a mixture of sappanwood and mangosteen peel as natural dyes in DSSC, an examination was conducted utilizing a UV-vis spectrophotometer with visible light wavelengths between 400–800 nm (Fig. 1) [33].

Based on the UV-vis spectrum image, the results of the measurement of the absorption area of pandan leaf and papaya leaf dyes contain chlorophyll-a. This is confirmed from previous research that chlorophyll-a shows maximum absorption at 665 nm and chlorophyll-b at 652 nm. The chlorophyll content in the dye can bind to TiO_2 so that it can increase efficiency through a faster energy conversion rate [34].

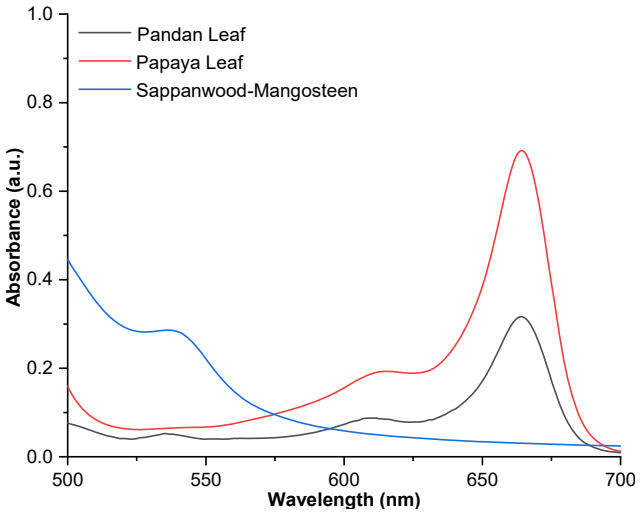

Fig 1. UV-vis spectra of papaya and pandan leaf dye and sappanwood bark-mangosteen peel

Conversely, a combination of dyes obtained from sappanwood and mangosteen peel displayed an absorption peak at 536.2 nm, affirming the existence of betacyanin content. The distinctive absorption pattern for the red-violet betalain group typically falls within the range from 535.0 to 540.0 nm, where it reaches its peak absorption [35]. Betalain compounds are phenolic substances that feature glycoside group substitutions in the ortho position and include a chromophore group, enabling a hydroxyl group to form a robust bond with the semiconductor material [36].

Voltammetry Cyclic Analysis

The important role of the band gap is to increase photocatalytic activity, which is associated with good electron transferability, an increase in light-harvesting, and an increase in catalytic active sites [37]. The CV method was employed to evaluate the band gap energy of each dye. This energy parameter was established based on the disparity between the HOMO and LUMO values [38]. Notably, the HOMO value corresponds to the oxidation state, represented by the oxidation peak, while the LUMO value is associated with the reduction state, signified by the reduction peak in the CV analysis [39]. The determination of HOMO, LUMO, and band gap energy values follows the Eq. (1-3) [40]:

$$E_{HOMO} = -(E_{ox} + 440)eV \quad (1)$$

$$E_{LUMO} = -e(E_{red} + 4.40)eV \quad (2)$$

$$E_g = E_{LUMO} - E_{HOMO} \quad (3)$$

Based on the band gap energy values obtained for each dye (Fig. 2 and Table 1), it shows that chlorophyll pigments from both papaya and pandan leaves as well as betacyanin pigments from the combination of sappanwood and mangosteen peel, can be used as natural dyes/sensitizers in DSSC because they meet the requirements of DSSC dyes. The LUMO values of each dye are significantly higher than the conduction value of TiO_2. It is essential for the dye to fulfill the requirement of having a sufficiently high LUMO level compared to the conduction band of the TiO_2 semiconductor, which is −4.0 eV [41-42] This allows the positioning of the LUMO dye energy to ensure sufficient driving force when electrons are injected into the semiconductor surface so that the dye regeneration process can take place in the DSSC [43-44].

The bandgap analysis conducted in this study reveals that the papaya leaf dye exhibits the smallest band gap (1.387 eV), followed closely by the secang-mangosteen dye (1.389 eV). The decreased band gap signifies an expanded absorption range as dye photon energy increases. The mechanism behind this phenomenon lies in the behavior of electrons, where a smaller band gap signifies the dye's capacity for facile electron transitions from lower-energy orbitals to higher-energy ones when exposed to light. Consequently,

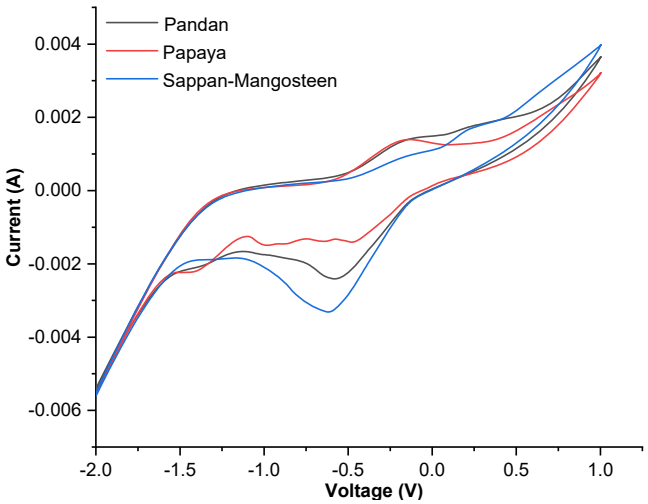

Fig 2. Cyclic voltammogram of papaya and pandan leaf dye and sappanwood bark-mangosteen peel

Table 1. Cyclic voltammetry parameter of the dye

Dye	Voltammetry cyclic		
	HOMO (eV)	LUMO (eV)	Band-gap (eV)
Pandan leaf	−4.29796	−2.91058	1.39600
Papaya leaf	−4.30489	−2.90907	1.38700
Sappanwood bark–Mangosteen peel	−4.29849	−2.90871	1.38900

this enhanced electron mobility translates into heightened sensitivity to light, rendering the dye remarkably adept at capturing solar energy [45]. This makes dyes such as papaya leaf and secang-mangosteen exceptionally well-suited for deployment in photovoltaic systems, including DSSCs.

SEM

Electrolyte-trapping polymers in the form of PVDF membrane and nanofiber were characterized using an SEM instrument. The characterization was conducted to ascertain the surface morphology and cross-sectional structure of the membrane. The characterization results were previously published in [16], showing that the PVDF and PVDF NF polymers have a diameter of 100–300 nm. Fig. 3 shows PVDF NF polymer has fibers with numerous pores, greater pore size, and lower density of particles than PVDF polymer. The payload transport in the DSSC system decreases in performance with increasing particle density. This happens because the greater the particle density level, the greater the force required to pass the particles so that the performance of the DSSC decreases. From the above explanation, it can be concluded that PVDF NF polymer has more potential to be applied as an electrolyte trapping polymer in DSSC systems than PVDF polymer [46-47].

Photovoltaic Studies

In this phase, the DSSC circuit is measured for open-circuit voltage (V_{oc}), short-circuit current (J_{sc}), fill factor (FF) and efficiency (η) using a multimeter under a 100 mW/cm^2 lamp intensity. The mechanism of the DSSC circuit occurs through several stages, namely the process of excitation of dye molecules so that dyes are produced in an oxidized state, reduction of electrolytes (I_3^- to I^-), oxidation of dyes (S^+ to S), energy transfer and recombination of dyes and electrons in the TiO_2 layer [9]. The equation used in the measurement is in Eq. (4) and (5) [48].

$$\eta = \frac{J_{sc} V_{oc} FF}{P_{in}} \quad (4)$$

$$FF = \frac{P_{max}}{J_{sc} V_{oc}} \quad (5)$$

Table 2 shows a clear difference in the effect of dye and electrolyte type on the measurement results in the form of V_{oc}, J_{sc}, FF and efficiency. In the context of this investigation, the energy conversion efficiency value serves as a crucial indicator, highlighting the DSSC's capacity to effectively convert solar energy into electrical energy [49]. Electrolytes play a major role as a step process for charge recombination at the TiO_2/dye/electrolyte interface which affects the ionic conductivity. The presence of polymer in the electrolyte can reduce the ionic conductivity of the DSSC circuit so that the results of the J_{sc} and V_{oc} produced decrease with the denser the polymer used. This happens because the density of the polymer can block the mobility of ions so that it inhibits the charge transfer process at the TiO_2/dye/electrolyte interface and the J_{sc} and V_{oc} values are increasingly decreasing from the liquid electrolyte, PVDF, and PVDF NF electrolyte (Fig. 4) [50-51].

Regarding the dyes, which play a crucial role in broadening the absorption spectrum of sunlight. In this study, papaya and pandan leaves were used with chlorophyll pigment content, while a mixture of sappan and mangosteen produced betacyanin pigments. Based on the information presented in the provided data, it is

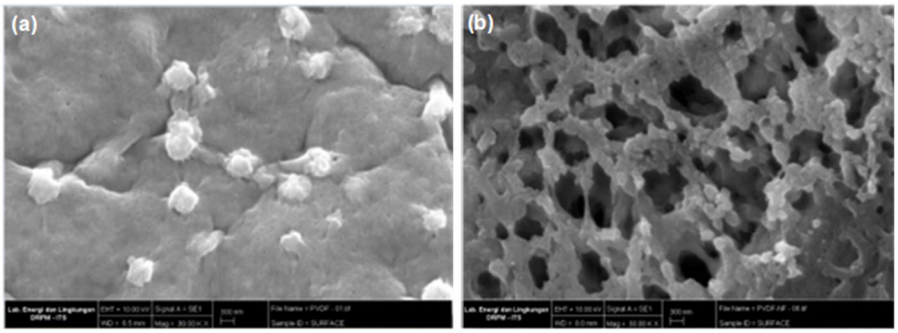

Fig 3. Membrane surface morphology 30.000× of (a) PVDF and (b) PVDF NF

Table 2. Photovoltaic parameters of the DSSC

No.	Dye	Electrolyte	J_{sc} (μA/cm^2)	V_{oc} (mV)	FF (%)	H (%)
		Liquid	3.1	390	40.4×10^{-2}	1.18
1.	P-M	PVDF NF	2.9	327	45.3×10^{-2}	0.93
		PVDF	2.7	308	42.1×10^{-2}	0.84
		Liquid	3.0	434	42.4×10^{-2}	1.31
2.	P_y-E	PVDF NF	2.7	393	44.1×10^{-2}	1.07
		PVDF	2.1	349	52.7×10^{-2}	0.72
		Liquid	3.1	401	63.5×10^{-2}	1.26
3.	SM-A	PVDF NF	3.0	391	57.1×10^{-2}	1.17
		PVDF	2.7	357	48.8×10^{-2}	0.95

P: pandan; P_y: papaya; SM: sappanwood-mangosteen; A: aquadest; M: methanol; E: ethanol; L: liquid electrolyte; NF: PVDF NF electrolyte; P: PVDF electrolyte

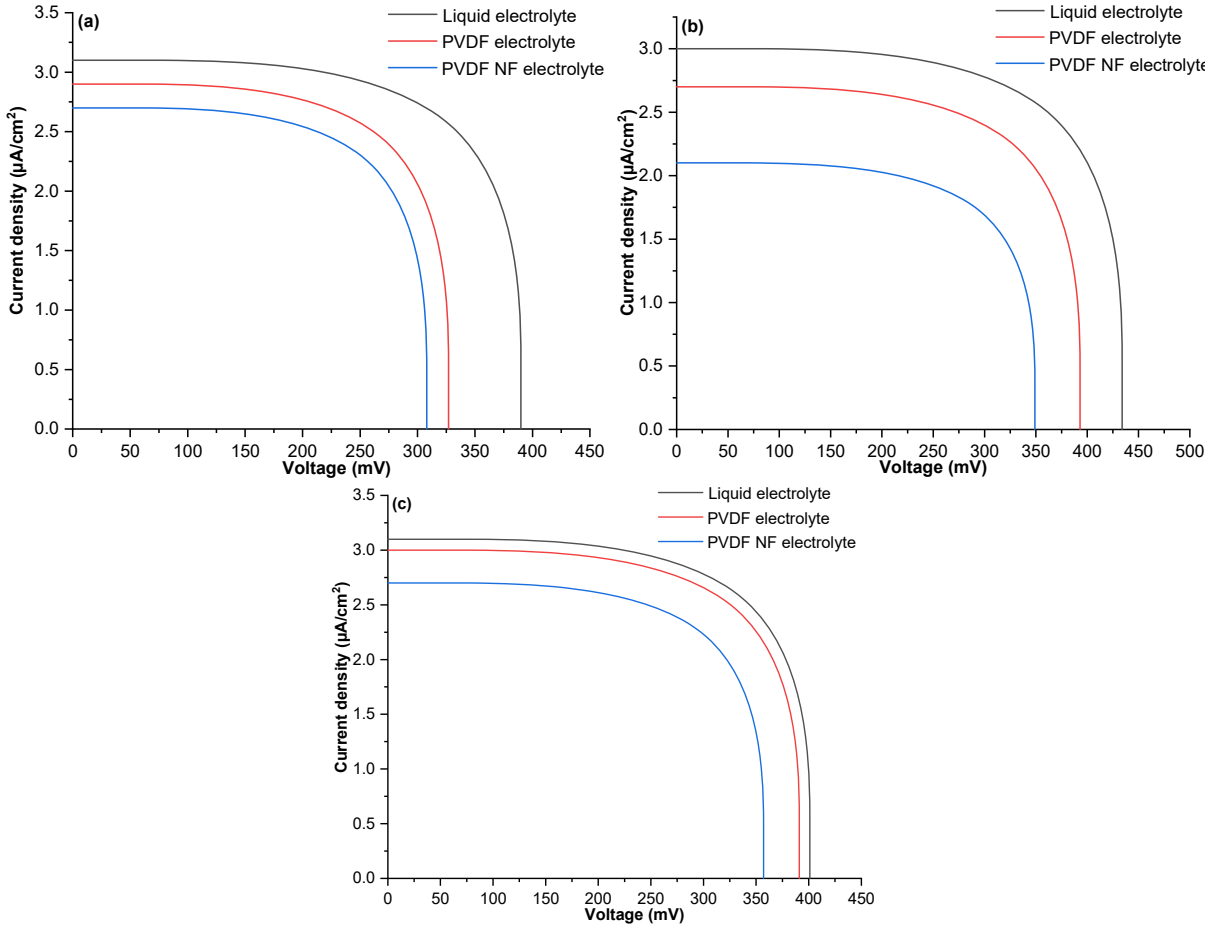

Fig 4. Photocurrent–voltage curve for DSSC sensitized by various extracts and electrolytes (a) P-M (b) P_y-E (c) SM-A

evident that papaya leaves exhibit superior efficiency when examined without the application of polymer electrolytes. On the other hand, the efficiency of secang-mangosteen dye with polymer electrolytes is notably higher. This observation is in alignment with the earlier band gap analysis, which indicated that the papaya dye has a smaller band gap, closely followed by the secang-mangosteen band gap value. The smaller the bandgap value, the faster the electron transfer will occur with the number of conjugated chains [52]. Chlorophyll pigment

has a major role in the photosynthesis process as the main capturing unit of sunlight. With the performance of DSSC from electron transfer in the form of sunlight, the possibility of regeneration runs faster [53]. In addition, chlorophyll is composed of a carboxylate group that could bind to TiO_2 so it plays a role in the conversion of energy for the better.

FTIR Analysis

Spectroscopic analysis of FTIR was employed to investigate the interaction of chemical complexes and structural properties, especially the membrane structure and the interaction of ions/polymers/solvents with electrolytes. Fig. 5 shows the spectrum comparison of FTIR analysis results on PVDF nanofiber and pure PVDF which is in the area 598.85–2984.63 cm^{-1}.

PVDF polymer exhibits four distinct crystalline phases, specifically referred to as α, β, γ, and δ. From many research, PVDF shows two peaks namely α-phase and β-phase. In the PVDF membrane, the α-phase showed an absorption peak of 762.71 cm^{-1}, while the β-phase was located at 841.15 and 873.09 cm^{-1}. The peak of 841.15 cm^{-1} also shows CH_2 rocking and asymmetric stretching of CF_2. Furthermore, the presence of peaks at 613.88 and 873.09 cm^{-1} was detected, indicating the occurrence of mixed-mode CF_2 bending and CCC skeletal vibrations [54]. Pure PVDF and bending of CH_2 were shown at the absorption peak of 873.09 cm^{-1}. Meanwhile, the peaks of 762.71 and 795.97 cm^{-1} are CH_2 rocking vibrations and CF_3 stretching vibrations, and the peak of 1066.92 cm^{-1} is CH bending [10,55]. Stretching CF is located at the peaks of 873.09, 975.61, 1182.17 and 2984.09 cm^{-1}, indicating asymmetric stretching. Among all the identified peaks, the most notable peak was observed at 975.61 cm^{-1}, indicating the prominent presence of the polymer's crystalline form [55]. In addition, there are several peaks of the amorphous phase, which can be observed in Fig. 5.

The FTIR analysis of PVDF nanofibers reveals a minor shift in the absorption peak, namely at the absorption peak of 875.84 cm^{-1} from the initial 873.09 cm^{-1} in pure PVDF. In addition, the crystal phase (α) nanofiber PVDF and the initial rocking vibration CH_2 on the pure PVDF located at 762.71 shifted to 740.40 cm^{-1} in the nanofiber PVDF. This may be due to the preferential orientation of the chains towards nanofibers which causes high crystallite levels in the electrospinning process and confirms the presence of hydrogen bonds and other molecular-level interactions [10]. Fig. 6 shows a comparative analysis of the FTIR spectra for PVDF nanofiber, liquid electrolyte, PVDF NF-electrolyte, and conventional gel electrolyte which can be concluded to be closely related to salt-polymer interactions. Fig. 6 depicts the vibrational bands related to the amorphous phase of the polymer, showcasing prominent peaks detected at 841.15 and 873.09 cm^{-1}.

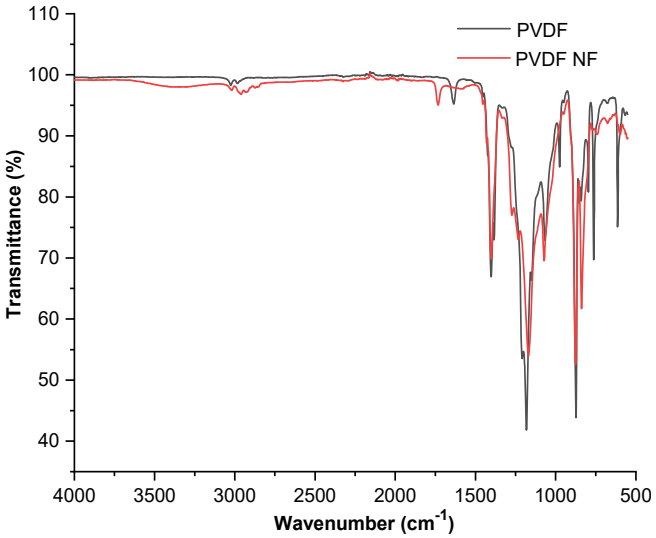

Fig 5. The result of FTIR analysis on PVDF nanofiber and pure PVDF is in the area 598.85–2984.63 cm^{-1}

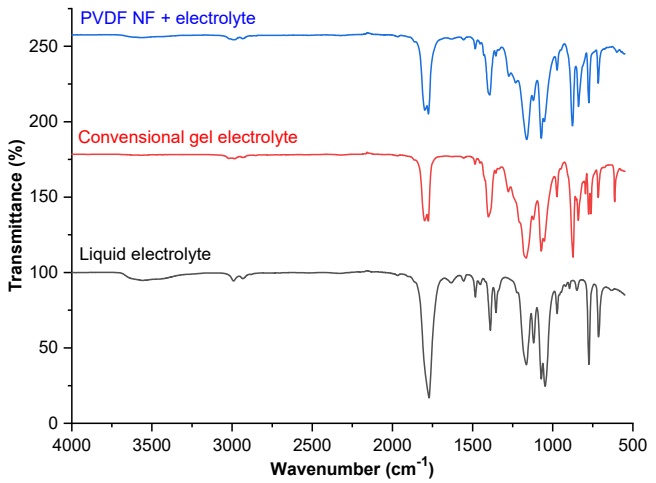

Fig 6. FTIR analysis results of PVDF nanofiber + electrolyte, gel, and liquid electrolyte

The interaction between the salt-polymer in the electrolyte can be understood by analyzing the β-phase peak of PVDF, as it becomes challenging to rely on other commonly observed peaks of the gel electrolyte phase. In pure PVDF the peaks of 841.15 and 873.09 cm^{-1} are the β-phase, which has a slight shift from 875.84 cm^{-1} in nanofiber PVDF, as seen in Fig. 7, due to their asymmetrical nature [10]. Meanwhile, after electrolytic immersion in pure PVDF, peaks were observed at 840.67 and 873.09 cm^{-1}, while in PVDF nanofibers peaks appeared at 839.15 and 876.88 cm^{-1}, which are CF stretching and a combination of CF_2 & CCC stretching vibrations, and CH_2 bending, CH_2 rocking, CF_2 asymmetric stretching [10,55]. The reduction in intensity of both peaks observed in both nanofiber-based and conventional gel-based electrolytes could be attributed to the dilution effect caused by the liquid component [10].

Fig. 7 shows two peaks, namely at the peak of 894 and 1066 cm^{-1}, which is the EC (Ring Breathe) which is only visible on the EC. The presence of the salt in the Li^+-EC system leads to the separation of the two peaks, indicating the interaction between K^+ and EC ions within the system [10]. In addition, basic cations are observed in the EC Raman spectrum in a similar frequency range. Thus, band separation like this can be said to be an energy shift corresponding to the deformation ring (breath). This is proportional to the induced polarization and the strength of polarization exhibited by K^+ ions, which is dependent on the electrical charge densities of the cations. Consequently, the obtained results tend to be smaller compared to those obtained with Li^+ [10]. In addition, EC also appears in electrolytes, liquid electrolytes are at peaks of 1071.44 and 861.74 cm^{-1}, conventional gel electrolytes appear at peaks of 1071.40 and 840.67 cm^{-1}, solid electrolytes are located at peaks of 1071.31 and 839.15 cm^{-1}.

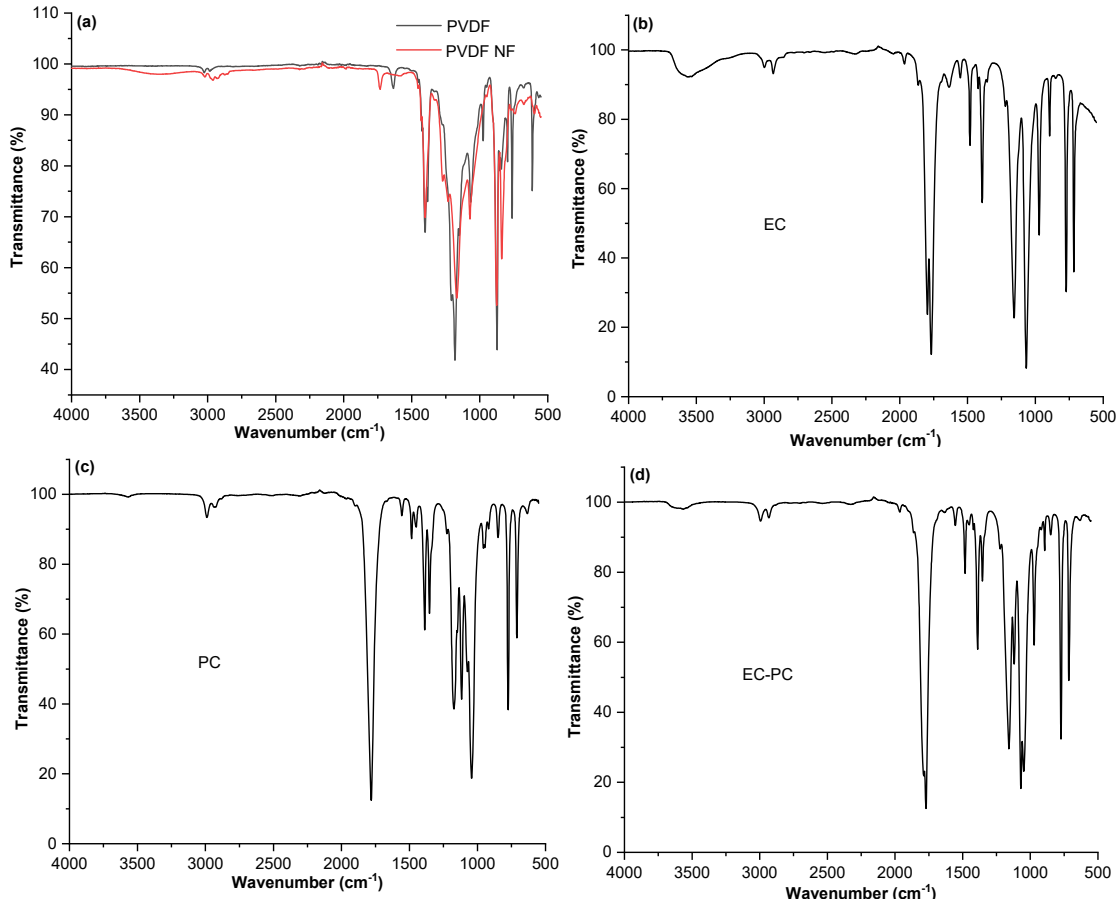

Fig 7. FTIR analysis spectrum of (a) pure PVDF, PVDF nanofiber (b) EC, (c) PC, and (d) EC-PC

Table 3. The absorption peaks of K^+ & EC complexes in liquid, conventional gel, and solid electrolytes

Absorption area specification	Liquid electrolyte (cm^{-1})	Conventional gel electrolyte (cm^{-1})	Solid electrolyte (cm^{-1})
K^+ & EC complex	895.20	873.09	876.88

Fig. 8 and Table 3 illustrate the interactions between EC and EC-K^+ absorption regions for different types of electrolytes. Considering the data, the conventional gel electrolyte exhibited the lowest peak at 873.09 cm^{-1} for the interaction between EC and K^+, while the highest peak was the liquid electrolyte at 895.2 cm^{-1}. This can happen because in the electrolyte nanofiber, K^+ ions are more bound to the EC so that the salt can easily dissociate leaving the glass iodide ion fraction free to carry out charge transport which results in a higher current of light compared to conventional gel electrolytes. While the liquid electrolyte has the highest peak due to the lack of a polymer matrix and its low viscosity. With low viscosity, it can produce the highest photocurrent so that cargo transportation is faster [10].

In the electrolyte, the amorphous phase polymer vibration band (β) is not very significant because in the polymer the amorphous phase peak (β) is related to the polymer solvent interactions in the electrolyte and the interactions between chains in the polymer. In addition, in electrolytes the amorphous phase (β) corresponds to the interactions of the replaced polymer chains [51].

DSC Analysis

Thermogravimetric characterization of PVDF membranes + electrolyte (PVDF + EI), PVDF nanofibers + electrolyte (PVDF NF + EI), PVDF membranes, ethylene carbonate (EC), and propylene carbonate (PC) was carried out using DSC (Linseis STA PT-1000). The characterization results previously published in previous research [16] which can be seen in Fig. 9, show that the melting temperature of PVDF NF + electrolyte is lower than that of PVDF + electrolyte. This is related to the crystallization of PVDF NF decreased by 2.19% compared to PVDF 2.31%.

From the characterization results, the thermal transition of polymers with or without electrolyte can reach 100 °C indicating high thermal stability for DSSC applications [56]. The broad endothermic peak observed

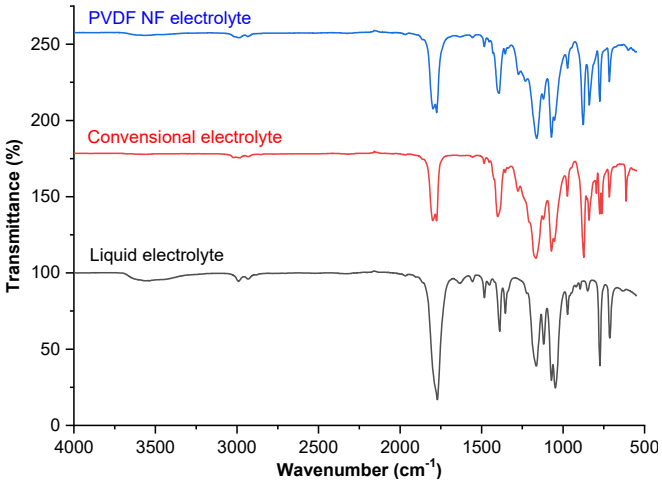

Fig 8. FTIR analysis of the electrolytes

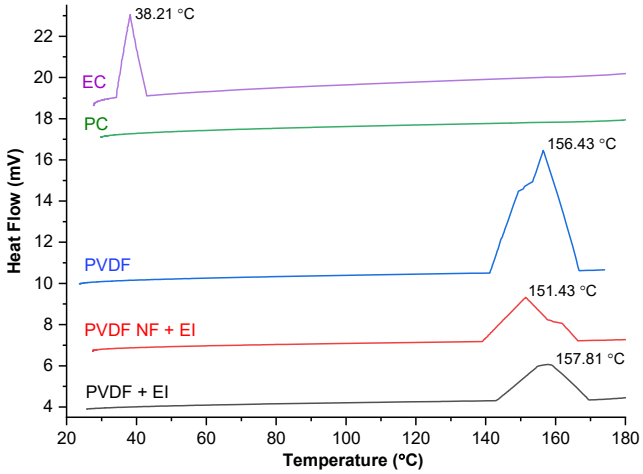

Fig 9. DSC thermograms of PVDF membranes + electrolyte, PVDF nanofibers + electrolyte, PVDF membranes, ethylene carbonate, and propylene carbonate at temperatures ranging from 25 °C to 180 °C

in Fig. 9, as depicted by the characterization results, indicates a close association with the melting points of the polymers present in the electrolyte [11].

■ CONCLUSION

This comprehensive study explored the potential of natural dyes extracted from pandan leaves, papaya leaves, and sappan-mangosteen for application in DSSCs. The presence of chlorophyll-a in pandan and

papaya leaves was confirmed through absorption peaks at 664.1 and 664.0 nm, respectively, while betacyanin was confirmed by a peak at 536.2 nm in sappan-mangosteen, highlighting their suitability for solar cell applications. Electrochemical analysis revealed promising energy band gaps, with papaya leaves showing the smallest band gap at 1.387 eV, closely followed by sappan-mangosteen at 1.389 eV, and pandan leaves at 1.396 eV. To address the significant challenge of electrolyte leakage in DSSCs, this study successfully introduced a PVDF polymer electrolyte. SEM analysis showed superior properties in PVDF NF, such as larger pores and lower particle density, contributing to enhanced performance. Furthermore, thermogravimetric analysis demonstrated high thermal stability in both PVDF and PVDF NF with electrolytes, withstanding temperatures up to 100 °C. Notably, papaya leaves achieved an outstanding 1.31% efficiency without a polymer electrolyte, while sappan-mangosteen reached 1.17% with PVDF NF and 0.95% with PVDF, comparable to a liquid electrolyte's 1.26% efficiency. This study offers valuable insights into natural dye utilization in DSSC technology and practical solutions for enhancing efficiency and stability with polymer electrolytes, contributing to greener energy solutions.

■ ACKNOWLEDGMENTS

The author would like to thank the Ministry of Education, Culture, Research, and Technology of the Indonesia Republic for providing financial support through national competitive research grants under Contract Number B/29547/UN38.III.1/LK.04.00/2023.

■ CONFLICT OF INTEREST

The authors have no conflict of interest.

■ AUTHOR CONTRIBUTIONS

Nafisatus Zakiyah, Nita Kusumawati, and Pirim Setiarso conducted the experiments. Nafisatus Zakiyah, Supari Muslim, and Qurrota A'yun performed calculations and data processing. Nafisatus Zakiyah, Qurrota A'yun, and Marinda Mayliansarisyah Putri drafted and revised the manuscript. All authors read and approved the final version of the manuscript.

■ REFERENCES

[1] Omar, A., Ali, M.S., and Abd Rahim, N., 2020, Electron transport properties analysis of titanium dioxide dye-sensitized solar cells (TiO_2-DSSCs) based natural dyes using electrochemical impedance spectroscopy concept: A review, *Sol. Energy*, 207, 1088–1121.

[2] Yeoh, M.E., Chan, K.Y., Wong, H.Y., Low, P.L., How Thien, G.S., Ng, Z.N., Ananda Murthy, H.C., and Balachandran, R., 2023, Hydrothermal duration effect on the self-assembled TiO_2 photo-anode for DSSC application, *Opt. Mater.*, 141, 113907.

[3] Estiningtyas, I.W., Kusumawati, N., Setiarso, P., Muslim, S., Rahayu, N.T., Safitri, R.N., Zakiyah, N., and Fachrirakarsie, F.F., 2023, Effect of natural dye combination and pH extraction on the performance of dye-sensitized photovoltaics solar cell, *Int. J. Renewable Energy Dev.*, 12 (6), 1054–1060.

[4] Chumwangwapee, N., Suksri, A., and Wongwuttanasatian, T., 2023, Investigation of bi-colour natural dyes potential for dye sensitized solar cell, *Energy Rep.*, 9, 415–421.

[5] Diantoro, M., Maftuha, D., Suprayogi, T., Reynaldi Iqbal, M., Solehudin, S., Mufti, N., Taufiq, A., Hidayat, A., Suryana, R., and Hidayat, R., 2019, Performance of *Pterocarpus indicus* Willd leaf extract as natural dye TiO_2-dye/ITO DSSC, *Mater. Today: Proc.* 17, 1268–1276.

[6] Abdalhadi, S.M., Al-Baitai, A.Y., and Al-Zubaidi, H.A., 2021, Synthesis and characterization of 2,3-diaminomaleonitrile derivatives by one-pot Schiff base reaction and their application in dye synthesized solar cells, *Indones. J. Chem.*, 21 (2), 443–451.

[7] Kusumawati, N., Setiarso, P., and Muslim, S., 2018, Polysulfone/polyvinylidene fluoride composite membrane: Effect of coating dope composition on membrane characteristics and performance, *Rasayan J. Chem.*, 11 (3), 1034–1041.

[8] Önen, T., Karakuş, M.Ö., Coşkun, R., and Çetin, H., 2019, Reaching stability at DSSCs with new type gel electrolytes, *J. Photochem. Photobiol., A*, 385, 112082.

[9] Tan, C.Y., Farhana, N.K., Saidi, N.M., Ramesh, S., and Ramesh, K., 2018, Conductivity, dielectric studies and structural properties of P(VA-*co*-PE) and its application in dye sensitized solar cell, *Org. Electron.*, 56, 116–124.

[10] Bandara, T.M.W.J., Weerasinghe, A.M.J.S., Dissanayake, M.A.K.L., Senadeera, G.K.R., Furlani, M., Albinsson, I., and Mellander, B.E., 2018, Characterization of poly(vinylidene fluoride-*co*-hexafluoropropylene) (PVdF-HFP) nanofiber membrane based quasi solid electrolytes and their application in a dye sensitized solar cell, *Electrochim. Acta*, 266, 276–283.

[11] Semalti, P., and Sharma, S.N., 2019, Dye sensitized solar cells (DSSCs) electrolytes and natural photo-sensitizers: A review, *J. Nanosci. Nanotechnol.*, 20 (6), 3647–3658.

[12] Sundaramoorhy, K., Muthu, S.P., and Perumalsamy, R., 2018, Enhanced performance of 4,4′-bipyridine-doped PVdF/KI/I_2 based solid state polymer electrolyte for dye-sensitized solar cell applications, *J. Mater. Sci.: Mater. Electron.*, 29 (21), 18074–18081.

[13] Bharati, D.C., Kumar, H., and Saroj, A.L., 2019, Chitosan-PEG-NaI based bio-polymer electrolytes: Structural, thermal and ion dynamics studies, *Mater. Res. Express*, 6 (12), 125360.

[14] Abisharani, J.M., DineshKumar, R., Devikala, S., Arthanareeswari, M., and Ganesan, S., 2020, Influence of 2,4-diamino-6-phenyl-1-3-5-triazine on bio synthesized TiO_2 dye-sensitized solar cell fabricated using poly(ethylene glycol) polymer electrolyte, *Mater. Res. Express*, 7 (2), 025507.

[15] Sahito, I.A., Ahmed, F., Khatri, Z., Sun, K.C., and Jeong, S.H., 2017, Enhanced ionic mobility and increased efficiency of dye-sensitized solar cell by adding lithium chloride in poly(vinylidene fluoride) nanofiber as electrolyte medium, *J. Mater. Sci.*, 52 (24), 13920–13929.

[16] Kusumawati, N., Setiarso, P., Santoso, A.B., Muslim, S., A'yun, Q., and Putri, M.M., 2023, Characterization of poly(vinylidene fluoride) nanofiber-based electrolyte and its application to dye-sensitized solar cell with natural dyes, *Indones. J. Chem.*, 23 (1), 113–126.

[17] Wu, X., Wu, Y., Chen, L., Yan, L., Zhou, S., Zhang, Q., Li, C., Yan, Y., and Li, H., 2018, Bioinspired synthesis of pDA@GO-based molecularly imprinted nanocomposite membranes assembled with dendrites-like Ag microspheres for high-selective adsorption and separation of ibuprofen, *J. Membr. Sci.*, 553, 151–162.

[18] Guo, F., Zhang, C., Wang, Q., Hu, W., Cao, J., Yao, J., Jiang, L., and Wu, Z., 2019, Modification of poly(vinylidene fluoride) membranes with aluminum oxide nanowires and graphene oxide nanosheets for oil-water separation, *J. Appl. Polym. Sci.*, 136 (20), 47493.

[19] Khumalo, N., Nthunya, L., Derese, S., Motsa, M., Verliefde, A., Kuvarega, A., Mamba, B.B., Mhlanga, S., and Dlamini, D.S., 2019, Water recovery from hydrolysed human urine samples via direct contact membrane distillation using PVDF/PTFE membrane, *Sep. Purif. Technol.*, 211, 610–617.

[20] Nthunya, L.N., Gutierrez, L., Lapeire, L., Verbeken, K., Zaouri, N., Nxumalo, E.N., Mamba, B.B., Verliefde, A.R., and Mhlanga, S.D., 2019, Fouling-resistant PVDF nanofibre membranes for the desalination of brackish water in membrane distillation, *Sep. Purif. Technol.*, 228, 115793.

[21] Deng, W., Zhao, H., Pan, F., Feng, X., Jung, B., Abdel-Wahab, A., Batchelor, B., and Li, Y., 2018, Response to comment on "Visible-light-driven photocatalytic degradation of organic water pollutants promoted by sulfite addition", *Environ. Sci. Technol.*, 52 (3), 1677–1678.

[22] Deng, W., and Li, Y., 2021, Novel superhydrophilic antifouling PVDF-BiOCl nanocomposite membranes fabricated via a modified blending-phase inversion method, *Sep. Purif. Technol.*, 254, 117656.

[23] Ahmad, N.A., Goh, P.S., Yogarathinam, L.T., Zulhairun, A.K., and Ismail, A.F., 2020, Current advances in membrane technologies for produced water desalination, *Desalination*, 493, 114643.

[24] Kusumawati, N., Setiarso, P., Sianita, M.M., and Muslim, S., 2018, Transport properties, mechanical behavior, thermal and chemical resistance of asymmetric flat sheet membrane prepared from PSf/PVDF blended membrane on gauze supporting layer, *Indones. J. Chem.*, 18 (2), 257–264.

[25] Kusumawati, N., Setiarso, P., Muslim, S., and Purwidiani, N., 2018, Synergistic ability of PSf and PVDF to develop high-performance PSf/PVDF coated membrane for water treatment, *Rasayan J. Chem.*, 11 (1), 260–279.

[26] Li, Y., Xu, M., Xia, Y., Wu, J., Sun, X., Wang, S., Hu, G., and Xiong, C., 2020, Multilayer assembly of electrospun/electrosprayed PVDF-based nanofibers and beads with enhanced piezoelectricity and high sensitivity, *Chem. Eng. J.*, 388, 124205.

[27] Liu, G., Tsen, W.C., Jang, S.C., Hu, F., Zhong, F., Zhang, B., Wang, J., Liu, H., Wang, G., Wen, S., and Gong, C., 2020, Composite membranes from quaternized chitosan reinforced with surface-functionalized PVDF electrospun nanofibers for alkaline direct methanol fuel cells, *J. Membr. Sci.*, 611, 118242.

[28] Liu, L., Xu, T., Gui, X., Gao, S., Sun, L., Lin, Q., Song, X., Wang, Z., and Xu, K., 2021, Electrospun silsequioxane-grafted PVDF hybrid membranes for high-performance rechargeable lithium batteries, *Composites, Part B*, 215, 108849.

[29] Moshfeghian, M., Azimi, H., Mahkam, M., Kalaee, M.R., Mazinani, S., and Mosafer, H., 2021, Effect of solution properties on electrospinning of polymer nanofibers: A study on fabrication of PVDF nanofibers by electrospinning in DMAC and (DMAC/acetone) solvents, *Adv. Appl. NanoBio-Technol.*, 2 (2), 53–58.

[30] Wang, H., Zhang, J., Ning, X., Tian, M., Long, Y., and Ramakrishna, S., 2021, Recent advances in designing and tailoring nanofiber composite electrolyte membranes for high-performance proton exchange membrane fuel cells, *Int. J. Hydrogen Energy*, 46 (49), 25225–25251.

[31] Han, Y., Shi, C., Cui, F., Chen, Q., Tao, Y., and Li, Y., 2020, Solution properties and electrospinning of polyacrylamide and ε-polylysine complexes, *Polymer*, 204, 122806.

[32] Hoseini, F.S., Taherian, R., and Atashi, A., 2021, Manufacturing and properties of polyvinyl alcohol/fibrin nanocomposite used for wound dressing, *Adv. Appl. NanoBio-Technol.*, 2 (1), 6–12.

[33] Ezike, S.C., Hyelnasinyi, C.N., Salawu, M.A., Wansah, J.F., Ossai, A.N., and Agu, N.N., 2021, Synergestic effect of chlorophyll and anthocyanin co-sensitizers in TiO_2-based dye-sensitized solar cells, *Surf. Interfaces*, 22, 100882.

[34] Ganta, D., Jara, J., and Villanueva, R., 2017, Dye-sensitized solar cells using aloe vera and cladode of cactus extracts as natural sensitizers, *Chem. Phys. Lett.*, 679, 97–101.

[35] García-Salinas, M.J., and Ariza, M.J., 2019, Optimizing a simple natural dye production method for dye-sensitized solar cells: Examples for betalain (*Bougainvillea* and beetroot extracts) and anthocyanin dyes, *Appl. Sci.*, 9 (12), 2515.

[36] Purushothamreddy, N., Dileep, R.K., Veerappan, G., Kovendhan, M., and Joseph, D.P., 2020, Prickly pear fruit extract as photosensitizer for dye-sensitized solar cell, *Spectrochim. Acta, Part A*, 228, 117686.

[37] Güzel, E., Arslan, B.S., Durmaz, V., Cesur, M., Tutar, Ö.F., Sarı, T., İşleyen, M., Nebioğlu, M., and Şişman, İ., 2018, Photovoltaic performance and photostability of anthocyanins, isoquinoline alkaloids and betalains as natural sensitizers for DSSCs, *Sol. Energy*, 173, 34–41.

[38] Vasanthi, D.S., Ravichandran, K., Kavitha, P., Sriram, S., and Praseetha, P.K., 2020, Combined effect of Cu and N on bandgap modification of ZnO film towards effective visible light responsive photocatalytic dye degradation, *Superlattices Microstruct.*, 145, 106637.

[39] Setiarso, P., Harsono, R.V., and Kusumawati, N., 2023, Fabrication of dye sensitized solar cell (DSSC) using combination of dyes extracted from curcuma (*Curcuma xanthorrhiza*) rhizome and binahong (*Anredera cordifolia*) leaf with treatment in pH of the extraction, *Indones. J. Chem.*, 23 (4), 924–936.

[40] Sinha, D., De, D., and Ayaz, A., 2018, Performance and stability analysis of curcumin dye as a photo sensitizer used in nanostructured ZnO based DSSC, *Spectrochim. Acta, Part A*, 193, 467–474.

[41] Çakar, S., Atacan, K., and Güy, N., 2019, Synthesis and characterizations of TiO_2/Ag photoanodes for used indigo carmine sensitizer based solar cells, *Celal Bayar Univ. J. Sci.*, 15 (1), 23–28.

[42] Khatun, N., Tiwari, S., Amin, R., Tseng, C.M., Biring, S., and Sen, S., 2020, Stable anatase phase with a bandgap in visible light region by a charge compensated Ga–V (1:1) co-doping in TiO_2, *Ceram. Int.*, 46 (7), 8958–8970.

[43] Lerrick, R.I., Bere, W., Braga, M.D.S., Supriyanto, A., and Essa, A.H., 2023, T-grafting BODIPY-based photosensitizers: The synthesis of 2,6-diethylacrylic-8-(*o*-methoxyphenyl)BODIPY and Its DSSC performance, *Indones. J. Chem.*, 23 (1), 232–241.

[44] Kathiravan, A., Khamrang, T., Velusamy, M., and Jaccob, M., 2021, Synthesis, density functional theory and sensitization of indole dyes, *Mater. Lett.*, 283, 128745.

[45] Cheng, P., and Yang, Y., 2020, Narrowing the band gap: The key to high-performance organic photovoltaics, *Acc. Chem. Res.*, 53 (6), 1218–1228.

[46] Tawary, M., Pontoh, J., and Momuat, L., 2019, Analsis kandungan klorofil pada beberapa jenis tanaman palma, *Jurnal Bios Logos*, 9 (2), 76–82.

[47] Prasad, G., Liang, J.W., Zhao, W., Yao, Y., Tao, T., Liang, B., and Lu, S.G., 2021, Enhancement of solvent uptake in porous PVDF nanofibers derived by a water-mediated electrospinning technique, *J. Materiomics*, 7 (2), 244–253.

[48] Elmorsy, M.R., Abdel-Latif, E., Badawy, S.A., and Fadda, A.A., 2020, Molecular geometry, synthesis and photovoltaic performance studies over 2-cyanoacetanilides as sensitizers and effective co-sensitizers for DSSCs loaded with HD-2, *J. Photochem. Photobiol., A*, 389, 112239.

[49] Adhitya, A., Rahmalia, W., Syahbanu, I., Gusrizal, G., and Adhitiyawarman, A., 2023, Deep eutectic solvent (DES) based on choline chloride and mono-, di-, poly-ethylene glycol as KI/I_2 electrolyte solvents on DSSC devices, *Indones. J. Chem.*, 23 (5), 1294–1303.

[50] Selvanathan, V., Yahya, R., Alharbi, H.F., Alharthi, N.H., Alharthi, Y.S., Ruslan, M.H., Amin, N., and Akhtaruzzaman, M., 2020, Organosoluble starch derivative as quasi-solid electrolytes in DSSC: Unravelling the synergy between electrolyte rheology and photovoltaic properties, *Sol. Energy*, 197, 144–153.

[51] Rao, B.N., Suvarna, R.P., and Raghavender, M., 2021, Synthesis of gel polymer electrolyte with PEO/RbI/I_2 for DSSC applications, *Mater. Today: Proc.*, 46, 4349–4355.

[52] Tractz, G., Viomar, A., Dias, B.V., de Lima, C.A., Banczek, E., da Cunha, M.T., Antunes, S.R.M., and Rodrigues, P.R.P., 2018, Recombination study of dye sensitized solar cells with natural extracts, *J. Braz. Chem. Soc.*, 30 (2), 371–378.

[53] Narender, B., Naveena, N.L., Pravalika, P., Kaleem, S., Vamshi, M.K., and Mandhadi, J.R., 2017, Pharmacological evaluation of root and leaf extracts of *Dracaena reflexa* var. *angustifolia*, *Innov Pharm Pharmacother*, 5 (3), 141–146.

[54] Lusiana, R.A., Indra, A., Prasetya, N.B.A., Sasongko, N.A., Siahaan, P., Azmiyawati, C., Wijayanti, N., Wijaya, A.R., and Othman, M.H.D., 2021, The effect of temperature, sulfonation, and PEG addition on physicochemical characteristics of PVDF membranes and its application on hemodialysis membrane, *Indones. J. Chem.*, 21 (4), 942–953.

[55] Saha, S., Yauvana, V., Chakraborty, S., and Sanyal, D., 2019, Synthesis and characterization of polyvinylidene-fluoride (PVDF) nanofiber for application as piezoelectric force sensor, *Mater. Today: Proc.*, 18, 1450–1458.

[56] Sharma, K., Sharma, V., and Sharma, S.S., 2018, Dye-sensitized solar cells: Fundamentals and current status, *Nanoscale Res. Lett.*, 13 (1), 381.